

# Bistable colloidal orientation near a charged surface

Mohit Singh and Yoav Tsori

*Department of Chemical Engineering, Ben-Gurion University of the Negev, Israel 8510501*

---

## Abstract

Anisotropic particles oriented in a specific direction can act as artificial atoms and molecules, and their controlled assembly can result in a wide variety of ordered structures. Towards this, we demonstrate the orientation transitions of uncharged peanut-shaped polystyrene colloids, suspended in a non-ionic aprotic polar solvent, near a flat surface whose potential is static or time-varying. The charged surface is coated with an insulating dielectric layer to suppress electric currents. The transition between several orientation states such as random, normal or parallel orientation with respect to the surface, is examined for two different colloid sizes at low-frequency ( $\sim 10 - 350$  kHz) or static fields, and at small electric potentials. In time-varying (AC) field, a detailed phase diagram in the potential-frequency plane indicating the transition between particles parallel or normal to the surface is reported. We next present the first study of orientation switching in static (DC) fields, where no electro-osmotic or other flow is present. A reversible change between the two colloidal states is explained by a theory showing that the sum of electrostatic and gravitational energies of the colloid is bistable. The number of colloids in each of the two states depends on the external potential, particle and solvent permittivities, particle aspect ratio, and distance from the electrode.

*Keywords:* Colloids, charged surface, bistability, electric field, torque

---

## 1. Introduction

The application of electric fields to suspensions of colloidal particles can lead to well-defined structures and ordered phases. Some of the ordered structures are potentially useful in electrochemistry [1], biosensors [2, 3], electronic displays [4, 5], photonics [6, 7, 8, 9] and electrical devices [10, 11]. Isotropic colloidal particles suspended in a medium can rapidly rearrange upon application of an alternating (AC) electric field [7]. In non-conducting fluids, this transition from random to regular arrangement depends strongly on the difference between the dielectric constants of colloidal particles and the suspending solution. The dielectric contrast induces dipole-dipole interactions, which lead to particles chaining one next to the other. The colloidal chains orient preferably in the direction of the external electric field. In some conditions, the intra-chain interactions render two-dimensional hexagonal particle arrays. Anisotropic particles can be

aligned in electric fields, whether hard or soft, charged or neutral. Neutral particles usually align parallel to the electric field because the dielectric anisotropy means that this is energetically favored. In charged particles, the electric dipole can be due to the migration of charges in one direction and the opposite migration of the counterions. For example, Yang *et al.* [12] reported the behavior, structure, and dynamics of charged asymmetric polystyrene dimers under an AC electric field applied perpendicularly to a substrate. They reported in-plane assemblies of the charged doublet, triplet, and quadruplet chiral clusters with applied low frequencies.

The effect of time-varying electric fields on colloidal orientation is commonly investigated at the high-frequency, MHz, range [13]. At such high frequencies, the electric double layer of residual ions in the solution vanishes, and electro-osmotic flow is negligible. The structure formation at the MHz range can be obtained by applying relatively high electric field strengths, which polarize the colloidal core and induce dipole-dipole interactions.

Much less attention has been paid to low-frequency electric fields, of the order of 10–100 kHz. At such low frequencies, several problems are encountered, such as abnormal alignment of colloids [14], clumps of rods and spheres [15], induction in phases, and instability of suspensions of long and thin colloidal chains [16, 17]. In the case of anisotropic colloids, short ellipsoidal rods tend to align parallel to each other [18]. However, the polarization of condensed ions, the double layer interaction, and electro-osmotic flow may hamper the colloidal alignment in low frequencies. Additionally, in such studies, the strength of the applied field is much lower than that used in the MHz range.

Recently, a theoretical work showed that an elongated colloid near a charged surface could be aligned with its long axis *parallel* or *perpendicular* to the field. The non-classical perpendicular orientation occurs only in spatially non-uniform fields. It results from a nontrivial torque that acts on the particle due to the presence of an electric double layer. When such a particle is found near a charged surface, the colloid orientation can thus switch between two states, depending on the surface potential, the distance from the surface, the colloid aspect ratio, and other factors [19]. Unlike the works reported in the literature [12, 20], we demonstrate orientation switching of large uncharged peanut-shaped colloids in the presence of small voltage and small or zero-field frequencies and negligible currents. A dilute and non-ionic colloidal solution is used in the experiments, leading to negligible inter-colloidal interaction. The study is focused on the colloids near the charged surface and away from colloidal aggregates, and hydrodynamic flow is absent. Thus, the forces acting on the colloids are thermal, electrical, and gravity. In this first-of-its-kind study, we experimentally demonstrate the orientation switching in the simultaneous presence of DC electric field and gravity. Experimental observations are explained using a unified theory.

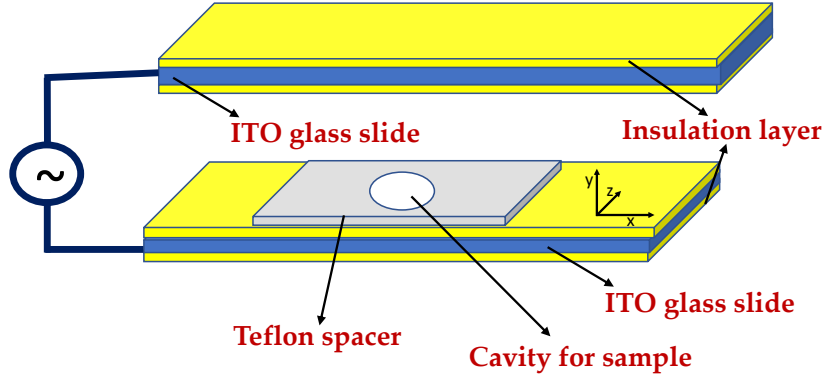


Figure 1: Schematic of the experimental setup used to study the colloid orientation switching in electric fields. An insulating tape (yellow) is used to prevent direct contact between the ITO-covered glass and the solution. The sample is observed directly by an optical microscope.

## 2. Experimental

### 2.1. Materials and methods

Two  $25 \times 75$  mm glass slides covered with a thin conducting ITO layer are used as electrodes. Electrically-neutral polystyrene peanut-shaped particles with reported dimensions of  $2.8 \times 4.1$  and  $5.1 \times 7.7 \mu\text{m}$  are purchased from Magsphere. Dimethyl sulfoxide (DMSO) (Sigma-Aldrich) is used as a solvent. Particle solutions of the two colloid sizes are prepared at a volume fraction of  $10^{-3}$  by sonicating the solution for 5 min before each experiment. A high-voltage power amplifier (Trek model PZ700-A) with voltages up to  $700 V_{\text{rms}}$  and arbitrary waveform generators (OR-X function generator 325) are used to generate sinusoidal signals of desired voltage. In static field experiments, DC voltage is applied using Keithley 2410 Source Measuring Unit (SMU) and Trek power amplifier 2210. A camera (Thorlabs camera 8050M-CL-TE) fitted onto the top of an inverted phase-contrast microscope (Olympus BX 53F) is used to visualize the colloids.

### 2.2. Experimental setup

The experimental setup is shown schematically in Fig. 1. Two ITO-covered glass slides are placed onto each other; they are separated by the non-conductive Teflon tape of thickness  $300 \mu\text{m}$ . Similar to the work of Kuijk *et al.* [21], both electrodes are covered with  $\approx 60 \mu\text{m}$  transparent non-conductive tape to avoid direct contact between electrodes and solution. Therefore the field is relatively small, and its direction is parallel to gravity. The resulting electrode spacing is  $\approx 420 \mu\text{m}$ . The suspension is kept inside a circular cavity with a diameter of 5 mm in the Teflon layer. A volume of  $30 \mu\text{L}$  solution is inserted into the cavity, and the top electrode is gently placed to avoid air bubbles. All four corners are clamped using a “crocodile” pin clip. The ITO-covered glasses are connected

via wires to the power supplies. A new device is prepared specifically for every experiment to ensure the cleanliness of the setup. In the case of AC fields, the ionic conductivity of the solution is below the measurement threshold. In experiments with DC potentials in the same setup, a fast transient current just after switching on is followed by a decay to zero current and a buildup of an electric double layer at the insulating tape.

### 2.2.1. Errors in the measurements

The distribution of colloid orientations is obtained from the microscopy images by analysis of the apparent aspect ratios with ImageJ software. At a given field of view, not all colloids appear in focus (see inset images in Fig. 3); some appear with asymmetrically blurred boundaries. This blurriness causes errors in the measurement of the apparent aspect ratio. Additionally, for hundreds of colloids in thousands of images, light intensity and contrast adjustments may lead to errors in the automatic boundary detection process. This results in  $\sim 4\%$  error in the aspect ratio measurements. From Eq. 1 (see below) it follows that there is an error of  $15^\circ$ – $20^\circ$  in the calculated tilt angle  $\theta$ .

## 3. Results and discussion

### 3.1. Colloidal orientation in AC fields

In the literature, the colloidal orientation in AC fields is generally studied for isotropic particles, with the exception of a few recent works [22, 15, 23, 24, 25, 26, 27, 28, 29, 20]. Kuijk *et al.* reported a para-nematic phase orientation of nanorods in the MHz and  $\sim 160$  kHz ranges [21]. Less attention is paid to anisotropic colloids in low-frequency AC fields [21, 12, 20]. Ma *et al.* [20] investigated the assembly of negatively charged colloidal dimers by applying low-frequency AC electric fields and reported that the assembly and orientation is a sensitive function of the frequency. They also explored the effect of the DC field on the assembly of anisotropic colloids for various salt concentrations and found no orientation switching. Unlike the previous works, here we use neutral anisotropic colloids and report orientation switching in the presence of both AC and DC fields. In the first part of the work, we investigate the orientation of anisotropic colloids in low-amplitude and low-frequency AC fields as a function of their size, applied frequency, and potential. We construct a phase diagram in the frequency-potential plane. Polystyrene peanut-shaped prolate ellipsoidal particles with an aspect ratio  $\sim 1.5$  are dispersed in DMSO at 1 wt%. In the geometry used by us, the electric field is approximately uniform throughout the sample. The application of alternating fields periodically polarizes the colloids according to the Maxwell-Wagner-O’Konski mechanism, which is analogous to polarization due to a contrast in dielectric properties but also accounts for the contrast in conductivity [30].

We noticed that low-frequency fields in the range of 7–350 kHz cause micron-sized colloids to orient rapidly with their long axis parallel to the field. Due to the uniformity of the field, electrophoretic or dielectrophoretic motion is

not observed, and colloidal orientation is independent of the distance from the charged surface. In static fields, distance matters, as is explained below.

The colloids are observed in-situ by phase-contrast microscopy as cross-sections in the  $x$ - $z$  plane at a variable distance  $y$  from the electrodes (see Fig.1). In the absence of an electric field, the colloidal particles are homogeneously distributed, with a slight tendency to settle down at the bottom surface due to the slight difference between the specific densities of the colloids and solvent. Their orientation is random due to their thermal energy. As we show below, as soon as the electric field is turned on above the cut-off field amplitude and frequency, the colloids aligned along the field's direction, as manifested by their nearly circular cross-sections. If the colloid density is sufficiently high, a few minutes after the application of the field, colloids start to order in chains along the field's direction. The chain formation is reversible; colloids lose orientation and are randomly distributed within a few seconds after switching off the field.

We imaged the colloid as projected onto the  $x$ - $z$  plane. In this plane, the ellipsoid is an ellipse whose apparent aspect ratio  $AR$  is the ratio between the projected semi-major and semi-minor axis. To extract the tilt angle  $\theta$  of the long axis of the ellipsoid with respect to the  $y$ -axis, the following formula is used:

$$AR = \sqrt{\left(\frac{b}{c}\right)^2 \cos^2 \theta + \left(\frac{a}{c}\right)^2 \sin^2 \theta}. \quad (1)$$

Here  $a > b > c$  are the semi-major axes of the prolate ellipsoid. When the angle is  $\theta = 0^\circ$ , the apparent aspect ratio is  $AR = b/c$ , while  $\theta = 90^\circ$  yields  $AR = a/c$  (ellipsoid is lying parallel to the surface). One can thus calculate  $\theta$  by measuring  $AR$  and using the known values of  $a$ ,  $b$ , and  $c$ .

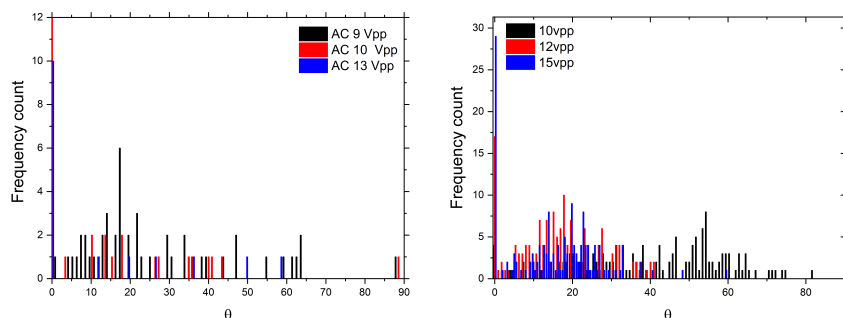


Figure 2: Distribution of colloid tilt angles  $\theta$  with respect to the  $y$  axis (normal to the electrodes), at fixed frequency and different applied voltages. Left:  $2.8 \times 4.1 \mu\text{m}$  sized colloids at 15 kHz frequency. Right:  $5.1 \times 7.7 \mu\text{m}$  sized colloids at 25 kHz frequency.

The colloid sample is injected between the electrodes, and voltage is applied. In Fig. 2 we show the measured colloidal orientation for two colloid sizes

at a fixed frequency and variable potentials. In the left panel, the colloids are smaller, and the field frequency is 15 kHz. At the small voltage of 9 V peak-to-peak (vpp), the electrostatic energy is not large enough to overcome thermal fluctuations, and the colloidal orientation remained random. At an increased voltage of 10vpp, the orientation shifted toward  $\theta = 0$ , and a more significant number of colloids are oriented vertically. Further increase in the voltage to 13vpp resulted in the vertical orientation of a vast majority of the colloids. The larger colloids showed a similar phenomenon, as shown in the right panel. At 10vpp, thermal energy overcomes the electrostatic energy, and the colloidal orientation is random, with a slight tendency toward  $\theta = 90^\circ$ , due to the gravitational force. At 12vpp, the distribution shifted to smaller values of  $\theta$ , while at 15vpp, this tendency became even more substantial. More significant potentials are required to orient the larger colloids since they are more affected by gravity. In these two cases, one would conclude that there are two threshold potentials, 10vpp and 12vpp, for the small and large colloids, respectively. We note that if colloids are treated as dipoles lying on a plane, their interaction force is inversely proportional to the fourth power of the distance between them (energy varies inversely with the cube of the distance) [20]. The colloidal interaction is therefore negligible for the dilute suspension used in the present experiments. Additionally, at an applied frequency of the order of  $10^4$  Hz, the electric torque is strong enough to align the colloids parallel to the applied field. As shown in Fig. 2, the colloidal orientation is random below a certain voltage because the electric torque is weak compared to the thermal noise.

We set out for a large-scale scan of the potential-frequency parameter space to generalize these observations. The results are summarized in Fig. 3. The colloidal orientation is determined from the peak apparent aspect ratio value at each value of potential and frequency. There is a line separating perpendicular and parallel orientations in the potential-frequency plane. At a fixed potential, an increase of frequency from small to large value across this line yields a transition from colloids parallel to the surface to perpendicular. The transition frequency is large at small potentials, while at high potentials, the transition is at small frequencies.

The phase diagram has two curves, black and red, corresponding to small and large particles, respectively. The larger the colloid, the more this curve is displaced upwards and to the right; one needs higher frequencies at given potentials or larger potentials at a given field. According to Jones [31], anisotropic particles align such that the effective energy

$$U = -\frac{1}{2} \text{Re}(\alpha_{\parallel} - \alpha_{\perp}) E^2 \cos^2(\theta) \quad (2)$$

is minimized. Here  $\alpha_{\parallel}$  and  $\alpha_{\perp}$  are the effective polarizabilities when particles are aligned parallel or perpendicular to the applied field, respectively, and  $\theta$  is the angle between long axis and the field. The polarizabilities are complex functions of the frequency, particle geometry and electrical properties of the solvent and particle. For higher aspect ratio and fixed voltage, one has to apply higher frequency to keep  $\text{Re}(\alpha_{\parallel} - \alpha_{\perp})$  positive. Interestingly, and not reported

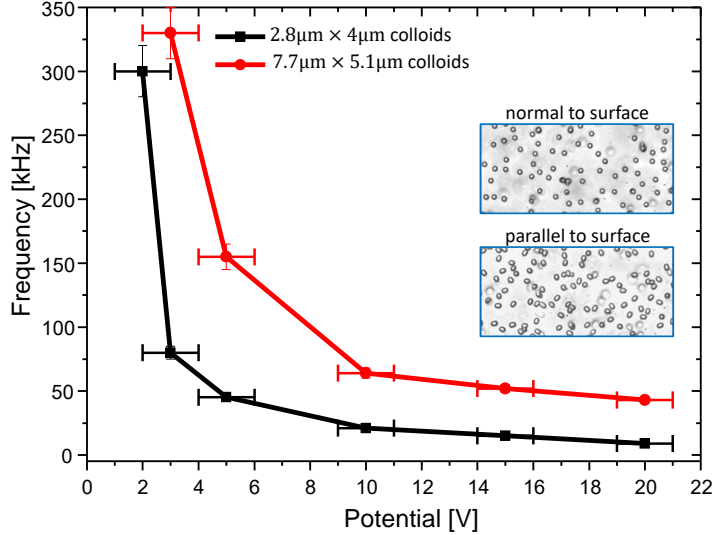


Figure 3: Phase diagram of colloidal orientation in AC electric fields. The lines signify a transition between two-particle orientations: below the line, particles are mainly parallel to the surface, while above it, they are perpendicular to it (parallel to the field). The black curve is the threshold for small particles, while the red curve is for bigger particles. An increase in either potential or frequency leads to particle orientation parallel to the field for both sizes. The inset images are representative microscope snapshots of the two colloidal states.

before, the threshold frequency varies non-linearly with applied potential. It should be noted that we performed experiments also without the insulation layer between the ITO electrode and the solvent. We found that the orientation threshold voltage is greatly reduced to the order of millivolts, but it is difficult to determine the transition value accurately.

### 3.2. Colloidal orientation in DC fields

In this part of the work, we checked the validity of the prediction that in constant potentials, colloidal orientation is bistable; namely, they would orient perpendicular or parallel to the surface, depending on the surface potential [19]. The “switching” behavior depends on the colloid size, dielectric constants of the colloid and solvent, and the distance from the surface. The driving force for colloidal orientation parallel to the surface is the ideal gas pressure exerted by dissolved ions. When the Debye screening length  $\lambda_D$  is comparable to the colloid size, this pressure varies significantly near the particle, with a large magnitude near one end and a small magnitude at the other end. In the present experiments, we have suspended 0.1 wt% of the bigger colloids, where image analysis is more accurate. The orientation angle is given in Eq. (1). As in the previous section, the error in the AR measurement is 5% because, experimentally, it is difficult to focus all colloids in a single frame, and the

inevitable blur results in inaccuracy in the value of AR. The distribution of AR is obtained by analyzing a single frame consisting of many colloids ( $\sim 10,000$ ) using the software ImageJ.

### 3.2.1. Electrostatic energy of a colloid near a charged surface

We calculated the electrostatic energy of a colloid near a charged surface,  $U_{es}$ , by modeling the colloid as a prolate ellipsoid with a semi-major axis  $a$  and semi-minor axes  $b$  and  $c < b$ . The electrode, located at  $y = -d$ , is covered by a thin dielectric insulating tape with thickness  $d$  and permittivity  $\varepsilon_d$ . The interface between dielectric and solvent is at  $y = 0$ , and the solvent, with permittivity  $\varepsilon_s$ , is found at  $y > 0$ .

**Effective potential in the solvent near an electrode covered with a dielectric.** In the experiments, the voltage  $V$  is applied on the metallic electrode, but the voltage the solvent “feels”,  $V_s$ , is considerably smaller. Once  $V_s$  is known, the distribution of the electric field near the colloid allows the calculation of forces acting on the colloid (see below). To find  $V_s$ , we first solved the Laplace and Poisson equations analytically *in the absence of colloid* as follows. We call  $\psi_d(y)$  and  $\psi_s(y)$  the electrostatic potentials in the dielectric and in the solvent, respectively. When ion densities are not too high, the potential  $\psi_s$  obeys the Poisson-Boltzmann equation

$$\nabla^2 \psi_s = \frac{en_0}{\varepsilon_s \varepsilon_0} \sinh\left(\frac{e\psi_s}{k_B T}\right). \quad (3)$$

Here  $n_0$  is the bulk ion density far from the charged wall and colloid,  $\varepsilon_0$  is the vacuum permittivity,  $e$  is the electron’s charge,  $k_B$  is the Boltzmann’s constant, and  $T$  is the absolute temperature. For high ion densities, such as in highly charged solutes or surfaces (e.g., in Langmuir monolayers), Eq.(3) can be modified by considering the finite size of the ions (for more details, see Refs. [32, 33]). The solution of this nonlinear equation in the semi-infinite region  $y \geq 0$  is

$$\frac{e\psi_s}{k_B T} = 2 \ln\left(\frac{1 + Be^{-y/\lambda_D}}{1 - Be^{-y/\lambda_D}}\right), \quad (4)$$

with the Debye screening length  $\lambda_D$  defined in

$$\lambda_D^2 = \frac{\varepsilon_s \varepsilon_0 k_B T}{2n_0 e^2}. \quad (5)$$

The variable  $B$  is given by

$$B = \frac{e^{\frac{eV_s}{2k_B T}} - 1}{e^{\frac{eV_s}{2k_B T}} + 1}, \quad (6)$$

where  $V_s = \psi_s(y = 0)$  depends on the experimental potential and needs to be found. Note that  $\psi_s(y \rightarrow \infty) = 0$  is obeyed. The electric field in the solvent is

$$-\frac{e\psi'_s(y)}{k_B T} = -\frac{1}{\lambda_D} \frac{4Be^{y/\lambda_D}}{B^2 - e^{2y/\lambda_D}}. \quad (7)$$



In the dielectric, the potential varies linearly, so that

$$\frac{e\psi_d(y)}{k_B T} = -\frac{eE_d}{k_B T}y + c, \quad (8)$$

where  $E_d = -\psi'_d$  is the field in the dielectric region. There are three variables  $c$ ,  $E_d$ , and  $V_s$  to be found and three conditions: (i) the continuity of potential across the dielectric-solvent interface at  $y = 0$ , the continuity of displacement field  $\varepsilon E$  across the interface, and (iii) the external potential at the electrode:

$$\begin{aligned} \psi_d(y=0) &= \psi_s(y=0) \\ -\varepsilon_d \psi'_d(y=0) &= -\varepsilon_s \psi'_s(y=0) \\ \psi_d(y=-d) &= V \end{aligned} \quad (9)$$

From the continuity of the potential at  $y = 0$ , one obtains  $c = eV_s/kT$ . The continuity of the displacement field implies that

$$\varepsilon_d \frac{eE_d}{kT} = -\frac{\varepsilon_s}{\lambda_D} \frac{4B}{B^2 - 1}$$

and hence

$$\frac{e\psi_d}{kT} = \frac{\varepsilon_s}{\varepsilon_d} \frac{1}{\lambda_D} \frac{4B}{B^2 - 1} y + \frac{eV_s}{kT}. \quad (10)$$

We finally go back to the equation for the total potential drop across the liquid and dielectric, that is,

$$-\frac{\varepsilon_s}{\varepsilon_d} \frac{d}{\lambda_D} \frac{4B}{B^2 - 1} + \frac{eV_s}{k_B T} = \frac{eV}{k_B T}. \quad (11)$$

This is a highly nonlinear equation for  $V_s$  as a function of  $V$ ,  $d/\lambda_D$ , and  $\varepsilon_s/\varepsilon_d$ . For sufficiently small external potentials, the Poisson-Boltzmann equation can be linearized. In this Debye-Hückel limit, one obtains that the ratio between the solvent and external potentials is approximately given by

$$\frac{V_s}{V} \approx \frac{\varepsilon_d \lambda_D}{\varepsilon_s d}, \quad (12)$$

and this ratio is small since  $\lambda_D/d$  is small.

Once  $V_s$  is known, whether in the nonlinear or linear regimes, it can be used as the boundary condition for the actual solution of the electric field *in the presence of a colloid* (below).

**Electrostatic forces acting on the colloid.** The electric field is given by the Laplace and Poisson equations in the dielectric colloid and in the solvent, respectively:

$$\begin{aligned} \varepsilon_c \tilde{\nabla}^2 \tilde{\psi} &= 0 && \text{inside the colloid} \\ \varepsilon_s \tilde{\nabla}^2 \tilde{\psi} &= \sinh(\tilde{\psi}) && \text{outside of the colloid} \end{aligned} \quad (13)$$

The potential  $\tilde{\psi} = e\psi/k_B T$  and lengths  $\tilde{\mathbf{r}} = \mathbf{r}/\lambda_0$  are now written as dimensionless quantities, where  $\lambda_0$  is given by  $\lambda_0^2 = \varepsilon_0 k_B T / 2n_0 e^2$ . Here  $\varepsilon_c$  and  $\varepsilon_s$  are the colloid and solvent permittivities, respectively. The boundary conditions for the potential are  $\tilde{\psi}(y=0) = eV_s/k_B T$  with  $V_s$  found from Eq. (11) and  $\tilde{\psi}(y \rightarrow \infty) = 0$ .

Once the electric field distribution is known, the forces on the colloid are found from the Maxwell stress tensor  $\mathbf{T}$  [34]:

$$\begin{aligned} \mathbf{T}_{ij} &= -p_0(n^\pm, T)\delta_{ij} + \frac{1}{2}\varepsilon_0\varepsilon E^2(-1 + \rho(\partial\varepsilon/\partial\rho)_T/\varepsilon)\delta_{ij} \\ &+ \varepsilon_0\varepsilon E_i E_j. \end{aligned} \quad (14)$$

$p_0$  is the ideal-gas pressure of the ions:  $p_0 = (n^+ + n^-)k_B T$ . The second term, depending on the colloid's density  $\rho$ , includes electrostriction. It can be lumped together with  $p_0$  without changing the forces on the colloid. The body force in the liquid  $\mathbf{f}$ , given as a divergence of the stress, and the force acting on a unit area of the interface between the colloid and the solvent,  $\mathbf{f}_s$ , are

$$\begin{aligned} \mathbf{f} &= -\nabla p_0 + \frac{1}{2}\nabla \left( \varepsilon_0 E^2 \rho \frac{\partial \varepsilon}{\partial \rho} \right)_T - \frac{1}{2}\varepsilon_0 E^2 \nabla \varepsilon + e(n^+ - n^-)\mathbf{E}, \quad (15) \\ \mathbf{f}_s &= \mathbf{T}\hat{n}, \quad (16) \end{aligned}$$

where  $\hat{n}$  is a unit vector perpendicular to the surface of the colloid.

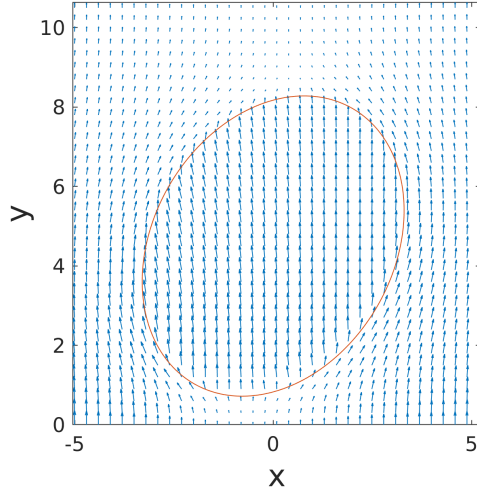


Figure 4: Representative electric field lines inside and outside of the colloid calculated numerically. The colloid is modeled as an ellipsoid (red line), tilted at an angle of  $\theta = 30^\circ$  with respect to the surface normal ( $y$ -direction). The charged surface is at  $y = 0$  and the solvent is at  $y > 0$  only. The field lines are the result of a numerical solution of Eqs. (13) in two spatial dimensions  $x$  and  $y$ . Lengths in  $x$  and  $y$  are scaled by  $\lambda_0$  (see text). In this and in other figures we used  $\varepsilon_c = 2.1$ ,  $\varepsilon_s = 48$ , and  $a = 4\lambda_0$ , and  $a/b = 1.32$ .

In the above formalism, one finds the electrostatic potential  $\tilde{\psi}$  and surface force  $\mathbf{f}_s$ , then integrates the total torque  $\tau(\theta) = \int_s \mathbf{r} \times \mathbf{f}_s ds$  over all elements of the colloid's surface  $ds$ . When the torque  $\tau(\theta)$  is known, the effective electrostatic rotational potential  $U_{\text{es}}(\theta)$ , is defined as

$$\tau(\theta) = -\frac{dU_{\text{es}}(\theta)}{d\theta}. \quad (17)$$

DMSO is used as a solvent because of its high dielectric constant  $\epsilon_s \approx 48$  and extremely low density of charge carriers. DMSO is a weak acid and, in contrast to water, the charges on the molecules are induced and not independent. From the density  $\rho = 1.1 \text{ g/cm}^3$  and molar mass  $m = 78.13 \text{ g/mol}$ , one obtains the volume of DMSO molecule as  $v_0 \approx 1.1 \times 10^{-22} \text{ cm}^3$ . The known pKa value of 35 allows to calculate the fraction  $f$  of charged molecules as  $f \sim 10^{-18}$ , which is well below the detection level of most measurement methods. The small residual ionic conductivity in DMSO is due to the unknown amount of impurities and leads to a Debye screening length  $\lambda_D$  of the order of one  $\mu\text{m}$ . The fact that the particle size is comparable to  $\lambda_D$  is meaningful for the physics of particle orientation – if an elongated particle is too small compared to  $\lambda_D$ , it “feels” a field that is effectively uniform, and it will orient parallel to the field. If the particle is too large compared to  $\lambda_D$ , the field decays too strongly near the surface and the particle does not feel significant forces.

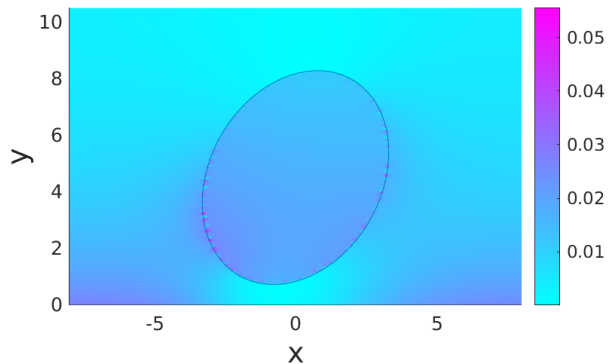


Figure 5: A plot of  $E^2(x, y)$  for the same colloid as in Fig. 4. Color bar expresses the intensity of field squared in dimensionless units. Lengths in  $x$  and  $y$  are scaled by  $\lambda_0$ . Here the surface potential is given by  $eV_s/k_B T = 1$ .

Figure 4 shows a representative numerical calculation of the field distribution in two spatial dimensions around the colloid. Field lines are derived from the potential  $\tilde{\psi}$  that we found from Eqs. (13). The surface at  $y = 0$  represents the dielectric-solvent interface, and its potential is  $\tilde{\psi} = \tilde{V}_s = eV_s/k_B T$ , with  $V_s$

taken as the solution of Eq. (11) with a particular value of electrode potential  $V$ . All lengths are scaled by  $\lambda_0$ . The field lines inside the colloid are nearly uniform; one may recall that the field lines inside a perfect dielectric ellipsoid are uniform if the external field is uniform. Here the external field is inherently nonuniform, resulting in deviations near the boundary of the colloid (red contour line).

The electrostatic force in Eq. (15) depends quadratically on the field. Figure 5 shows the distribution of field intensity  $E^2(x, y)$  inside and near the same colloid as in Fig. 4. The field's intensity is somewhat diminished between the colloid and the surface ( $x \approx 0, 0 \leq y \leq 1$ ) and sufficiently far from the surface ( $y \geq 6$ ). In these two figures, the tilt angle is  $\theta = 30^\circ$ ; to obtain  $U_{\text{es}}(\theta)$ , we repeated the calculation for a series of  $\theta$  values in the range  $0 \leq \theta \leq 90^\circ$ .

### 3.2.2. Gravitational energy of the colloid

In addition to the electrostatic energy of the colloid, we needed to add the gravitational energy of a tilted ellipsoid. The height of the center of mass of the ellipsoid above the surface as a function of the tilt angle  $\theta$  of the long axis with respect to the normal to the surface,  $h(\theta)$ , is

$$h(\theta) = \sqrt{b^2 \sin^2 \theta + a^2 \cos^2 \theta}. \quad (18)$$

When  $\theta = 0$ , the colloid is normal to the surface and the height of the center of mass is  $h = a$ ; when the ellipsoid is lying parallel to the surface,  $\theta = 90^\circ$  and  $h = b$ . The effective energy for the displacement of the center of mass of the ellipsoid is  $U_g = V \Delta \rho g h$ , where  $V = (4\pi/3)abc$  is the ellipsoid's volume,  $\Delta \rho$  is the density difference between the colloid and the surrounding solvent, and  $g$  is the gravitational acceleration. We thus find

$$U_g(\theta) = \frac{4\pi}{3} abc \Delta \rho g \sqrt{b^2 \sin^2 \theta + a^2 \cos^2 \theta}. \quad (19)$$

This energy is minimal when the colloid lies with its long axis parallel to the surface. It is instructive to estimate the order of magnitude of  $U_g$ . For a  $\mu\text{m}$ -sized colloid with  $a = b = c = 4 \mu\text{m}$  and  $\Delta \rho = 1 \text{ kg/m}^3$ , we have  $U_g \approx k_B T$ , and thus for colloids of similar size the gravitational energy is not negligible compared to the thermal energy.

Figure 6 shows the dimensionless electrostatic  $\tilde{U}_{\text{es}} = U_{\text{es}}/k_B T$  (top) and gravitational  $\tilde{U}_g = U_g/k_B T$  (bottom) energies vs. colloid tilt angle. At small surface potentials (value in legend),  $\tilde{U}_{\text{es}}$  has a global minimum at  $\theta = 0$ , indicating that colloids tend to orient parallel to the field and normal to the surface. When the potential increases, the minimum becomes deeper. However, due to the ‘‘ideal gas’’ pressure of ions and its nonuniform distribution near the surface, this behavior is non-monotonous – if the potential increases further, the global minimum becomes local, and the global minima appear at  $\theta = \pm 90^\circ$  (both orientations are equivalent), indicating that the most stable colloid orientation is parallel to the surface. As the voltage increases, the local minimum at  $\theta = 0$  completely disappears. The dependence of  $\tilde{U}_g$  is independent of voltage and its minimum is always at  $\theta = \pm 90^\circ$ .

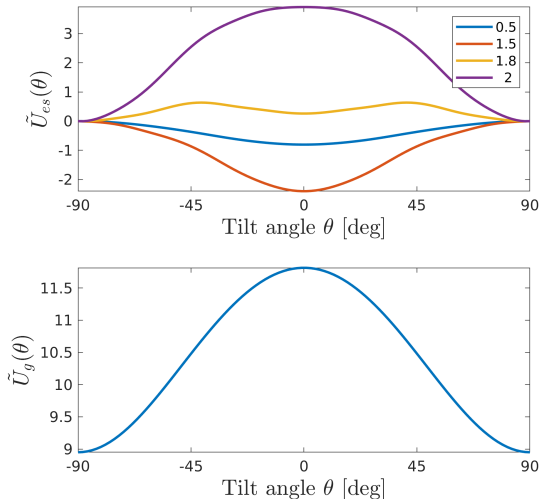


Figure 6: Top: Colloid’s electrostatic energy as a function of its tilt angle  $\theta$ ,  $\tilde{U}_{es} = U_{es}/k_B T$  with  $U_{es}$  defined in Eq. (17), for different external potentials. Legend shows the scaled surface potential  $eV_s/k_B T$ . Bottom: Scaled colloid potential energy due to gravity vs.  $\theta$ :  $\tilde{U}_g = U_g/k_B T$  with  $U_g$  from Eq. (19). We used  $b = 5.1 \mu\text{m}$ ,  $a = 6.7 \mu\text{m}$ ,  $c = b$ ,  $\Delta\rho = 1 \text{ kg/m}^3$ , and the ratio between the length in the  $z$  direction and  $l_{B0}$  is 5, where  $l_{B0} = e^2/(4\pi\epsilon_0 k_B T)$ .

The sum of electrostatic and gravitational contributions to the energy,  $\tilde{U}_{tot} = \tilde{U}_{es} + \tilde{U}_g$ , is plotted in Fig. 7. At small values of  $\tilde{V}_s$ , the gravitational part dominates the energy and the global minima are at  $\theta = \pm 90^\circ$ . As the potential increases, the electrostatic minimum is large enough and the global minimum shifts to  $\theta = 0$  (colloid normal to the surface). Further increase of  $\tilde{V}_s$  leads to re-stabilization of the minima at  $\theta = \pm 90^\circ$ .

In the experiments, the colloids are “polydisperse”, with an average value of the aspect ratio  $a/b$  and a finite probability for larger or smaller values. To account for this, we assumed that  $a$  obeys a normal distribution, that is, the probability of having  $a$  is given by  $P(a) = \exp(-(a - a_{av})^2 / 2a_{sd}^2) / \sqrt{2\pi a_{sd}^2}$ , where  $a_{av}$  is the average value and  $a_{sd}$  is the standard deviation. We made extensive numerical calculations of  $U(\theta) = U_{es}(\theta) + U_g(\theta)$  for all values of  $\theta$  and for three values of  $a$ :  $a = 1.27b$ ,  $a = 1.32b$ , and  $a = 1.37b$ . For a given value of  $a$ , the apparent aspect ratio AR as a function of  $\theta$  is given by Eq. (1). The relative frequency of colloids at angle  $\theta$  associated with this value of  $a$  is proportional to the Boltzmann weight  $\exp(-U(\theta))$ . We then calculated the value of  $U(\theta)$  for *all* values of  $a$  by interpolating  $U(\theta)$  from the three exact values, with the correct weight  $P(a)$  using  $a_{av} = 1.32b$  and  $a_{sd} = 0.03b$ . The total relative frequency of occurrence of AR is the sum of frequencies from all possible values of  $a$ .

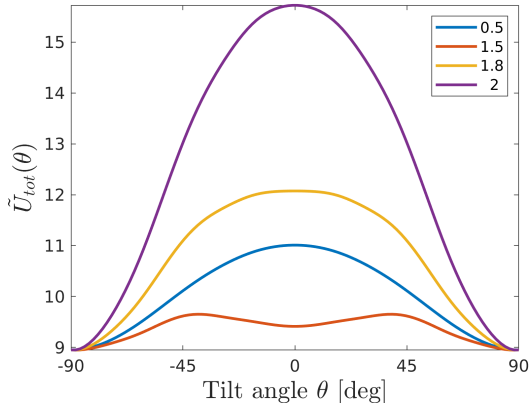


Figure 7: The sum of electrostatic and gravitational energies,  $\tilde{U}_{tot} = \tilde{U}_{es} + \tilde{U}_g$  from Fig. 6 for different surface potentials  $\tilde{V}_s = eV_s/k_B T$  (legend).

The experiments and theory are displayed in Fig. 8. The top panel shows the relative frequency of the apparent aspect ratio as observed experimentally in a sample of  $\sim 10,000$  particles. Different curves relate to the different voltages indicated in the legend. The  $y$ -axis is normalized such that the integral of each curve is unity. For all voltages, the maxima of the distribution are found at  $AR \sim 1.32$ , which corresponds to the ratio  $a/c$  of the ellipsoid, indicating particles lying flat at the surface. A smaller peak appears at small voltages around  $AR = 1.05$ . This corresponds to the ratio  $b/c$  of the ellipsoid, indicating colloids oriented normal to the surface (parallel to the field). The dependence of this peak on potential is non-monotonic – the peak height increases with increasing potentials and then decreases. The measurements are in equilibrium – an increase or decrease of the voltage followed by a return to the original value always leads to the same particle distribution. The theoretical results (bottom panel) show the same behavior semi-quantitatively. In particular, the theory predicts a large peak at  $AR \approx 1.32$  and a smaller peak at  $AR \approx 1.05$ , which disappears at large voltages.

#### 4. Conclusions

We studied the bistability of elongated ellipsoidal particles in time-varying AC and static DC electric fields. Two parallel ITO glass slide electrodes produced the field. The external frequency is a convenient handle that allows tuning the range of the interaction exerted by the charged surface (electrode)

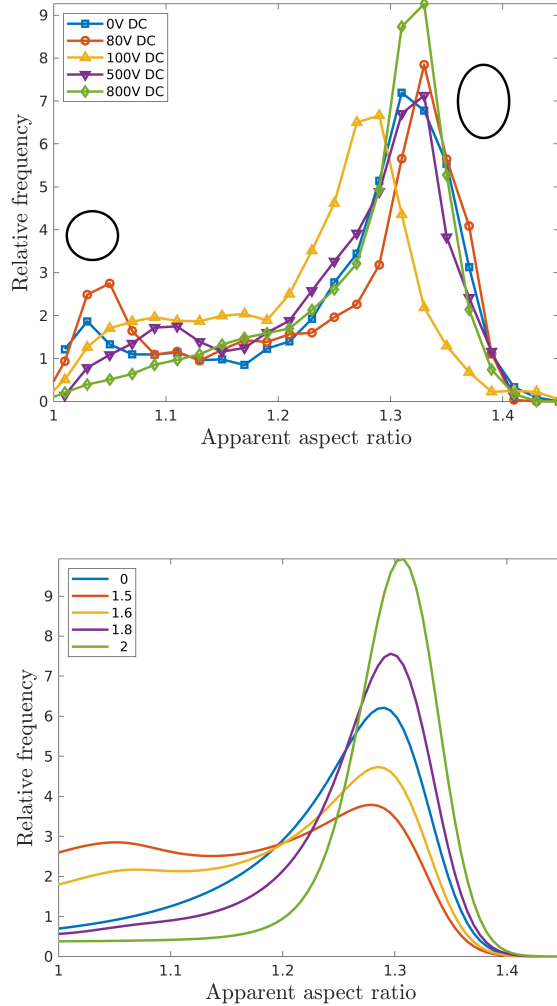


Figure 8: Top: Apparent aspect ratio AR distribution for colloids near the charged surface in DC fields (electrode potential  $V$  is indicated in the legend). The relative frequency is calculated by counting all the particles with a certain aspect ratio and dividing by the total number of particles ( $\sim 10,000$ ). Circle and ellipse illustrations indicate vertical and horizontal particle orientations, respectively. Bottom: Theoretical results corresponding to the top panel. Legend shows the dimensionless surface potential  $\tilde{V}_s$  calculated by Eq. (11) for a given value of  $V$ . We used  $a = 4\lambda_0$ , and the center-of-mass distance of the colloid from the  $y = 0$  surface is  $4.5\lambda_0$ .

on the particles; the potential determines the amplitude of the interaction. In the first part, we used AC fields at the above-kHz frequency, where the field is effectively spatially uniform. This is the limit where the influence of the surface has an infinite range. The extensive mapping of the large potential–frequency

parameter space is absent from previous works. The phase diagram in the potential–frequency plane is divided by a line into two regions. At low surface potentials, particles lay parallel to the surface. An increase of the frequency above the threshold line leads to their alignment normal to the surface. At large surface potential, the same transition happens but at a smaller threshold frequency. For larger particles, this line is displaced to larger potentials and frequencies (see Fig. 3).

While in AC fields, the force acting on the particles is spatially uniform, in DC fields, the physical picture is very different: here, screening occurs, and the field is substantial only sufficiently close to the electrode. Thus, the forces acting on a particle can be drastically different on the side near the electrode compared to the remote side. Because the particles are nonspherical, they feel a torque. Theory shows that this torque depends on the potential, location, tilt angle, and particle shape (given mainly by the ratio  $a/b$  of the two ellipsoidal axes). We extended the previous theory to include the effect of gravity, coupling to the difference between the specific densities of particles and solvent, and favoring particles lying flat on the surface. We verified experimentally the theoretical prediction that particle orientation is bistable, with a discontinuous first-order transition between particle orientation parallel to the surface to normal orientation.

The current study may have applications in various areas, such as in the fabrication of 3D non-corrosive and lower band-gaps with diamond-like lattice photonic crystals from anisotropic particles. It may help mimicking atoms and molecules with diverse geometry, chemical composition, and surface functionalities. Another interesting direction is related to plasmonics – it is well known that plasmons have different wavelengths parallel to the long or short axis of elongated particles. The switching behavior discovered here may allow for tuning the plasmon frequency of a colloidal array on a surface between two states. The present study advances the fundamental understanding of the forces acting on particles in electrolytes in electric fields. It serves as a first step toward a study of more complex phenomena that occur when such particles pack in high densities on a surface, where steric interactions are dominant.

It would be interesting to extend the current work to frequencies lower than the kHz range. At these frequencies, the distance dissolved ions traverse during one field cycle can be large, and Joule heating can be substantial. There is a fundamental question on the effect of this heating on the phenomena we observed here, especially recalling that heating would be more pronounced near the surface compared to far from it. Another, more application-oriented direction, is the possibility of controlling the optical properties of a surface: if the colloidal density is sufficiently large, we speculate that radiation impinging on the liquid-crystalline-like surface could be scattered, reflected, or polarized, depending on the orientation of the colloids.



## Acknowledgement

This work was supported by the Israel Science Foundation (ISF) grant No. 274/19.

## References

- [1] J. Ghoroghchian, S. Pons, M. Fleischmann, Gas phase electrochemistry on dispersions of microelectrodes, *J. Electroanal. Chem. Interfacial Electrochem.* 317 (1-2) (1991) 101–108.
- [2] O. Velev, E. Kaler, In situ assembly of colloidal particles into miniaturized biosensors, *Langmuir* 15 (11) (1999) 3693–3698.
- [3] K. F. Hoettges, M. B. McDonnell, M. P. Hughes, Use of combined dielectrophoretic/electrohydrodynamic forces for biosensor enhancement, *J. Phys. D: Appl. Phys.* 36 (20) (2003) L101.
- [4] B. Comiskey, J. D. Albert, H. Yoshizawa, J. Jacobson, An electrophoretic ink for all-printed reflective electronic displays, *Nature* 394 (6690) (1998) 253–255.
- [5] R. A. Hayes, B. J. Feenstra, Video-speed electronic paper based on electrowetting, *Nature* 425 (6956) (2003) 383–385.
- [6] Y. A. Vlasov, X.-Z. Bo, J. C. Sturm, D. J. Norris, On-chip natural assembly of silicon photonic bandgap crystals, *Nature* 414 (6861) (2001) 289–293.
- [7] S. O. Lumsdon, E. W. Kaler, O. D. Velev, Two-dimensional crystallization of microspheres by a coplanar ac electric field, *Langmuir* 20 (6) (2004) 2108–2116.
- [8] I. Hosein, M. Ghebrebrhan, J. Joannopoulos, C. Liddell, Dimer shape anisotropy: A nonspherical colloidal approach to omnidirectional photonic band gaps, *Langmuir* 26 (3) (2010) 2151–2159.
- [9] J. A. Schuller, E. S. Barnard, W. Cai, Y. C. Jun, J. S. White, M. L. Brongersma, Plasmonics for extreme light concentration and manipulation, *Nat. Mater.* 9 (3) (2010) 193–204.
- [10] K. D. Hermanson, S. O. Lumsdon, J. P. Williams, E. W. Kaler, O. D. Velev, Dielectrophoretic assembly of electrically functional microwires from nanoparticle suspensions, *Science* 294 (5544) (2001) 1082–1086.
- [11] J.-C. Bradley, H.-M. Chen, J. Crawford, J. Eckert, K. Ernazarova, T. Kurzeja, M. Lin, M. McGee, W. Nadler, S. G. Stephens, Creating electrical contacts between metal particles using directed electrochemical growth, *Nature* 389 (6648) (1997) 268–271.

- [12] X. Yang, N. Wu, Change the collective behaviors of colloidal motors by tuning electrohydrodynamic flow at the subparticle level, *Langmuir* 34 (3) (2018) 952–960.
- [13] J. Dhont, K. Kang, Electric-field-induced polarization and interactions of uncharged colloids in salt solutions, *Eur. Phys. J. E* 33 (1) (2010) 51–68.
- [14] H. Kramer, C. Graf, M. Hagenbüchle, C. Johner, C. Martin, P. Schwind, R. Weber, Electro-optic effects of aqueous fd-virus suspensions at very low ionic strength, *J. De. Phys. II* 4 (6) (1994) 1061–1074.
- [15] F. Mantegazza, M. Caggioni, M. Jiménez, T. Bellini, Anomalous field-induced particle orientation in dilute mixtures of charged rod-like and spherical colloids, *Nat. Phys.* 1 (2) (2005) 103–106.
- [16] K. Kang, J. K. Dhont, Double-layer polarization induced transitions in suspensions of colloidal rods, *Europhys. Lett.* 84 (1) (2008) 14005.
- [17] K. Kang, J. K. Dhont, Electric-field induced transitions in suspensions of charged colloidal rods, *Soft Matter* 6 (2) (2010) 273–286.
- [18] J. P. Singh, P. P. Lele, F. Nettekheim, N. J. Wagner, E. M. Furst, One- and two-dimensional assembly of colloidal ellipsoids in ac electric fields, *Phys. Rev. E* 79 (5) (2009) 050401.
- [19] Y. Tsori, Bistable colloidal orientation in polar liquid near a charged wall, *J. Colloid Interface Sci.* 559 (2020) 45–50.
- [20] F. Ma, S. Wang, L. Smith, N. Wu, Two-dimensional assembly of symmetric colloidal dimers under electric fields, *Adv. Funct. Mater.* 22 (20) (2012) 4334–4343.
- [21] A. Kuijk, T. Troppenz, L. Filion, A. Imhof, R. Van Roij, M. Dijkstra, A. Van Blaaderen, Effect of external electric fields on the phase behavior of colloidal silica rods, *Soft Matter* 10 (33) (2014) 6249–6255.
- [22] M. Mittal, E. M. Furst, Electric field-directed convective assembly of ellipsoidal colloidal particles to create optically and mechanically anisotropic thin films, *Adv. Funct. Mater.* 19 (20) (2009) 3271–3278.
- [23] A. F. Demirors, P. M. Johnson, C. M. van Kats, A. van Blaaderen, A. Imhof, Directed self-assembly of colloidal dumbbells with an electric field, *Langmuir* 26 (18) (2010) 14466–14471.
- [24] S. Hernandez-Navarro, J. Iñes-Mullol, F. Sagues, P. Tierno, Role of anisotropy in electrodynamically induced colloidal aggregates, *Langmuir* 28 (14) (2012) 5981–5986.
- [25] J. Yan, A. Rashidi, C. L. Wirth, Single and ensemble response of colloidal ellipsoids to a nearby ac electrode, *Colloids Surf. A: Physicochem. Eng. Asp.* 606 (2020) 125384.

- [26] R. S. Hendley, I. Torres-Díaz, M. A. Bevan, Anisotropic colloidal interactions & assembly in ac electric fields, *Soft Matter* 17 (40) (2021) 9066–9077.
- [27] B. W. Kwaadgras, T. H. Besseling, T. J. Coopmans, A. Kuijk, A. Imhof, A. Van Blaaderen, M. Dijkstra, R. Van Roij, Orientation of a dielectric rod near a planar electrode, *Phys. Chem. Chem. Phys.* 16 (41) (2014) 22575–22582.
- [28] M. Mohammadimasoudi, Z. Hens, K. Neyts, Full alignment of dispersed colloidal nanorods by alternating electric fields, *RSC Adv.* 6 (61) (2016) 55736–55744.
- [29] J. J. Crassous, A. M. Mihut, E. Wernersson, P. Pfeleiderer, J. Vermant, P. Linse, P. Schurtenberger, Field-induced assembly of colloidal ellipsoids into well-defined microtubules, *Nat. Commun.* 5 (1) (2014) 1–7.
- [30] H. Morgan, N. G. Green, *AC Electrokinetics: Colloids and Nanoparticles*, no. 2, Research Studies Press, 2003.
- [31] T. Jones, *Electromechanics of particles*, Cambridge University Press, Cambridge, (1995).
- [32] S. Ringe, *First-principles modeling in poisson-boltzmann electrolytes*, Ph.D. thesis, Technische Universität München (2017).
- [33] I. Borukhov, D. Andelman, H. Orland, Steric effects in electrolytes: a modified poisson-boltzmann equation,, *Phys. Rev. Lett.* 79 (3) (1997) 435.
- [34] W. K. H. Panofsky, M. Phillips, *Classical Electricity and Magnetism*, second ed., Dover Publications, 2005.